Analyst

Cite this: *Analyst*, 2012, **137**, 4584

www.rsc.org/analyst

PAPER

A simple and highly efficient route to the synthesis of $NaLnF_4$–Ag hybrid nanorice with excellent SERS performances†

Maofeng Zhang,[ab] Aiwu Zhao,*[ab] Da Li,[a] Henghui Sun,[a] Dapeng Wang,[a] Hongyan Guo,[a] Qian Gao,[a] Zibao Gan[a] and Wenyu Tao[a]

Received 6th June 2012, Accepted 3rd August 2012
DOI: 10.1039/c2an35758e

This paper reports the synthesis of a new class of $NaLnF_4$–Ag (Ln = Nd, Sm, Eu, Tb, Ho) hybrid nanorice and its application as a surface-enhanced Raman scattering (SERS) substrate in chemical analyses. Rice-shaped $NaLnF_4$ nanoparticles as templates are prepared by a modified hydrothermal method. Then, the $NaLnF_4$ nanorice particles are decorated with Ag nanoparticles by magnetron sputtering method to form $NaLnF_4$–Ag hybrid nanostructures. The high-density Ag nanogaps on $NaLnF_4$ can be obtained by the prolonging sputtering times or increasing the sputtering powers. These nanogaps can serve as Raman 'hot spots', leading to dramatic enhancement of the Raman signal. The $NaLnF_4$–Ag hybrid nanorice is found to be robust and is an efficient SERS substrate for the vibrational spectroscopic characterization of molecular adsorbates; the Raman enhancement factor of Rhodamine 6G (R6G) absorbed on $NaLnF_4$–Ag nanorice is estimated to be about 10^{13}. Since the produced $NaLnF_4$–Ag hybrid nanorice particles are firmly fastened on a silicon wafer, they can serve as universal SERS substrates to detect target analytes. We also evaluate their SERS performances using 4-mercaptopyridine (Mpy), and 4-mercaptobenzoic acid (MBA) molecules, and the detection limit for Mpy and MBA is as low as 10^{-12} M and 10^{-10} M, respectively, which meets the requirements of the ultratrace detection of analytes. This simple and highly efficient approach to the large-scale synthesis of $NaLnF_4$–Ag nanorice with high SERS activity and sensitivity makes it a perfect choice for practical SERS detection applications.

1. Introduction

Surface-enhanced Raman scattering (SERS) has attracted ever increasing attention due to its high sensitivity, specificity, and fingerprint effect in the detection of a variety of molecules.[1–4] Silver nanocrystals with well-defined and controllable shapes are employed as SERS-active substrates because of their remarkable plasmonic properties and resulting unique SERS performances.[5] This SERS effect has enabled its ability to detect a wide variety of analytes at extremely low concentrations even down to the single-molecular level.[6,7] To date, great efforts have been devoted to synthesizing different topologies, compositions, and surface structures of Ag nanocrystals. The most critical aspect of performing these SERS applications is the fabrication of SERS-active substrates with large SERS enhancement, high sensitivity, fine uniformity, good reproducibility, and biocompatibility.[8,9]

Recently, particular emphasis has been focused on the development of novel nanostructured SERS substrates with reliable and excellent sensing performance.[10–15] Typically, nanorice is a new hybrid nanoparticle geometry that combines the intense local fields of nanorods with the highly tunable plasmon resonances of nanoshells. The highly tunable nanorice plasmons essentially arise from plasmon hybridization between a metallic spheroid and an ellipsoidal nanocavity. The excitation of the longitudinal nanorice plasmon gives rise to enormous local field enhancements exploitable for SERS. Therefore, various methods have been developed to immobilize noble metals onto diverse supports to obtain the desired rice-shaped nanomaterials and explore their SERS properties. For instance, colloidal Au seed crystals were attached onto the spindle-shaped hematite nanoparticle cores by functionalizing the surface of the Fe_2O_3 core with 3-aminopropyl trimethoxysilane (APTMS). The gold seeds were then grown to form a continuous and complete Au shell layer.[16] Alternatively, with the assistance of an intermediate layer of SiO_2, Au/Ag was precipitated onto a spindle-shaped Fe_2O_3 core to produce nanorice particles[17] or the self-assembly and seeding method was used for silver plating of the proposed Fe_2O_3@Au-seed substrate to obtain the rice-like nanoparticles (NPs).[18] Such obtained nanomaterials show intriguing properties

[a]*Institute of Intelligent Machines, Chinese Academy of Sciences, Hefei, 230031, P. R. China. E-mail: awzhao@iim.ac.cn*
[b]*State Key Laboratory of Transducer Technology, Chinese Academy of Sciences, Hefei, 230031, P. R. China*
† Electronic supplementary information (ESI) available. See DOI: 10.1039/c2an35758e

and promising applications. However, their synthetic process may suffer from drawbacks such as the use of toxic reagents, multiple steps, high fabrication costs, or the need for special technicians to deal with it. Thus, the green, facile and cheap fabrication of SERS substrates on a large scale, while maintaining a high enhancement factor (EF) to detect single molecules and excellent reproducibility of the signal intensity, still remains challenging.

More recently, there has also been renewed interest in applying green chemistry principles to produce noble metal nanomaterials.[19,20] As a result, some green and sustainable methods have been largely developed for the synthesis of Au and Ag nanomaterials. Such as the preferred use of sonochemical methods,[21] microwave methods,[22] laser ablation,[23] and aqueous solvent.[24] Templating against hard (solid) templates is arguably the most effective and certainly the most common method for synthesizing rice-shaped Au- and Ag-NPs. For example, a method for coating rice-shaped iron oxide nanoparticles as templates with a thin gold shell to produce rice-shaped Au core–shell nanoparticles was devised;[16] Zhang and co-workers developed an efficient and green strategy to fabricate Au(Pt)-functionalized α-Fe_2O_3 hybrid nanospindles;[25] Zhao *et al.* introduced a new approach that combines the self-assembly and seeding methods for silver plating onto an Fe_2O_3@Au-seed substrate to form rice-shaped nanoparticles.[26] Unfortunately, even with their success in producing SERS-active substrates, the above-mentioned methods generally employ Fe_2O_3 as a core template to fabricate a metal hybrid SERS substrate. Moreover, the synthesis process may introduce complicated coupling agents (such as a silane coupling agent, or biomolecules) for linking the metal NPs onto the core surface. These coupling agents may bring extra interferential bands in the SERS measurements, especially if the target analytes have a similar Raman spectral response to the coupling agents. To tackle this problem, physical sputtering was exploited as a simple and direct means without introducing any coupling agents, for example, 3D hybrid silver nanocluster-decorated ZnO nanowire arrays were fabricated *via* depositing Ag nanoclusters onto ZnO nanowire arrays by using a gas-aggregation-type nanocluster beam source;[27] and the fabrication of arrays of vertically aligned cone-shaped ZnO nanorods decorated with Ag NPs as a highly sensitive and uniform 3D SERS substrate *via* ion-sputtering.[28] However, it is still necessary to explore other materials as templates to synthesize hybrid nanostructures directly.

Interestingly, rare-earth fluoride NPs with high chemical stability, high biocompatibility and low toxicity have been investigated for luminescence enhancement by Ag or Au.[29–32] For example, $NaYF_4$:Yb/Tm nanoparticles were surface-decorated with 1–2 nm Au seeds, increasing the emission intensity by 2.5 times;[33] and $NaYF_4$:Yb/Er nanocrystals assembled with gold nanospheres achieved a plasmon-enhanced upconversion enhancement factor of 3.8.[34] By contrast, further growth and coalescence of these Au islands led to the formation of an Au shell, which can greatly suppress the emission, possibly due to the strong scattering of excitation irradiation. These findings open a new pathway to rationally modulate the emission and quenching, and can open up new opportunities for energy harvesting and conversion. Inspired by this thought, using rare-earth fluoride NPs as the energy donor and gold or silver nanoparticles as the energy acceptor, to synthesize $NaLnF_4$–Ag hybrid nanostructures as SERS-active substrates is very likely a feasible and alternative strategy.

In this paper, we report the controlled synthesis of $NaLnF_4$–Ag hybrid nanorice particles as highly efficient SERS-active substrates, together with the characterization of their morphologies and optical properties. The obtained $NaLnF_4$–Ag nanorice particles are stable and can be large-scale produced with high repeatability and good uniformity. The resulting new hybrid nanorice generates abundant and high density 'hot spots' (formed within the interstitial crevices present in the metallic nanostructures), which leads to a high SERS sensitivity to Rhodamine 6G (R6G) that a concentration as low as 10^{-17} M can still be identified. More importantly, the produced hybrid nanorice particles are firmly fastened on the surface of a silicon wafer and can be used as a SERS-active substrate to directly detect target analytes without post-processing. And this kind of substrate can be fabricated in any silicon wafer to produce large areas of SERS substrates at a minimal cost. Thus, this facile, low-cost, and green chemistry-synthesized and highly sensitive hybrid SERS substrate shows a very promising and practical solution to the rapid ultratrace detection of analytes.

2. Experimental

2.1. Sample preparation

Materials. All of the chemical reagents are of analytical grade and used without further purification. Rare-earth chloride ($LnCl_3$), ethylenediaminetetraacetic acid (EDTA), and sodium fluoride (NaF) were purchased from the Shanghai Chemical Reagent Company.

Fabrication of rice-shaped $NaLnF_4$ nanoparticles. The rice-shaped $NaLnF_4$ nanoparticles were synthesized through a modified hydrothermal method.[35] In a typical procedure, 1 mmol of the hydrated $LnCl_3$ and 1 mmol of EDTA were dispensed into 40 mL of deionized water and magnetically stirred for 10 min. Then 12 mmol NaF was added dropwise to the above solutions and the mixture was constantly stirred for 10 min. Then the mixture was transferred into a 60 mL Teflon-lined stainless steel autoclave. The autoclave was sealed and maintained in an electric oven at 120 °C for 12 h, and then cooled to room temperature naturally. The products were carefully collected and washed with distilled water and absolute ethanol several times to remove impurities. Finally, the products were redispersed in 2 mL ethanol for further use.

Synthesis procedures of the $NaLnF_4$–Ag hybrid nanorice. Magnetron sputtering was applied to assemble Ag NPs onto the surface of the rice-shaped $NaLnF_4$ NPs using a magnetron sputter. First, homogeneous crystalline rice-shaped $NaLnF_4$ nanoparticles were ultrasonically dispersed in a mixed solvent, and transferred to the surface of a silicon wafer (2 cm × 2 cm), yielding a self-assembled monolayer. Next, after being dried in the air, the silicon wafer was placed in the magnetron sputtering chamber (2 cm away from the Ag target) to allow the sputtering of small Ag nanoparticles. The sputtering was operated for different periods of time or with different power levels. Lastly,

the as-prepared samples were cut into pieces (2 mm × 2 mm) as SERS substrates. These SERS substrates were immersed in Rhodamine 6G (R6G), 4-mercaptopyridine (Mpy), and 4-mercaptobenzoic acid (MBA) solutions of different concentrations for 12 h. The pieces were taken out, rinsed with ethanol and deionized water, and dried in air before the subsequent characterization.

2.2. Characterization

The morphologies of the samples were observed with field-emission scanning electron microscope (FESEM) images on a JEOL JSM-6300F SEM instrument. Transmission electron microscope (TEM) studies were performed with a JEOL-2010 microscope operated at an accelerating voltage of 200 kV with a tungsten filament. The UV/vis absorption spectra of the samples were recorded with a Shimadzu DUV-3700 spectrophotometer. The Raman scattering spectra were recorded on a confocal microprobe Raman system (Renishaw, inVia) with an excitation wavelength of 532 nm. During SERS measurements, the laser light was projected vertically onto the samples with a resultant beam diameter of about 4 μm. The excitation power is 0.5 mW and the integration time was 6 s for each spectrum. Twelve spectra were acquired for each of the measurements, and the average one was selected for figure legends. The spectra in this paper were background subtracted.

3. Results and discussion

Fig. 1 gives a schematic of the fabrication of the rice-shaped $NaLnF_4$ NPs decorated with Ag NPs on silicon wafers. Details are provided in the Experimental section. Fig. 1B–E shows SEM and corresponding TEM images of the products obtained under various conditions. It can be seen that a small amount of Ag NPs were assembled onto the surface of the rice-shaped $NaLnF_4$ NPs to form a thin silver shell within a short sputtering time. By prolonging the sputtering time, a mass of Ag NPs wsd decorated onto the surface of the $NaLnF_4$ NPs to achieve a more sensitive SERS substrate loaded with sufficient 'hot spots'. The SEM image indicates that the particles had a rice-like morphology, which is more or less similar to that of the hematite–Au core–shell nanorice particles reported by Halas and co-workers.[16] They had a hematite core with average lengths of 340 ± 20 nm and diameters of 54 ± 4 nm. Different from the case of hematite–Au nanorice particles, the cores of the present hybrid nanorice particles were rare-earth fluorides with an average length of 200 ± 7 nm and a diameter of 56 ± 3 nm. Although the rice-shaped $NaLnF_4$ NPs prepared with the present method could not be fully coated with Ag NPs (coverage of about 80–90%) to form complete core–shell nanostructures, the high SERS sensitivity makes them meet the requirements for the ultratrace detection of analytes as discussed below.

3.1. The particle size and morphology of the rice-shaped $NaLnF_4$ nanoparticles

Fig. 2A–F shows typical FESEM images of the $NaLnF_4$ nanoparticles synthesized through a modified hydrothermal method. Fig. 2A a is low-magnification SEM image of the rice-shaped $NaNdF_4$ nanoparticles. It clearly reveals that a large quantity and good uniformity of $NaNdF_4$ nanoparticles are achieved using this approach. It is also clear from Fig. 2B that the as-obtained nanoparticles have a highly monodisperse distribution

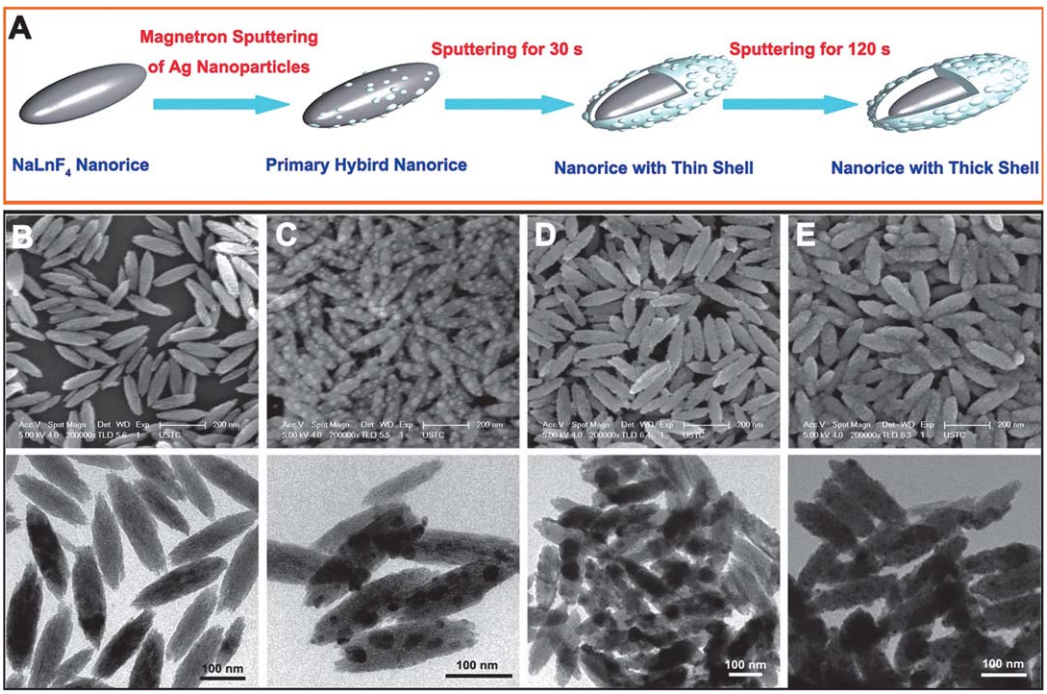

Fig. 1 (A) Schematic image of the fabrication of rice-shaped $NaLnF_4$ NPs decorated with Ag NPs on silicon wafers. FESEM (upper) and TEM (lower) images of (B) $NaLnF_4$ core (average length 200 ± 7 nm and diameter 56 ± 3 nm, (C) primary hybrid nanomaterials, (D) nanorice with thin shells (3.0 ± 1.7 nm), and (E) nanorice with thick shells (17.1 ± 0.7 nm).

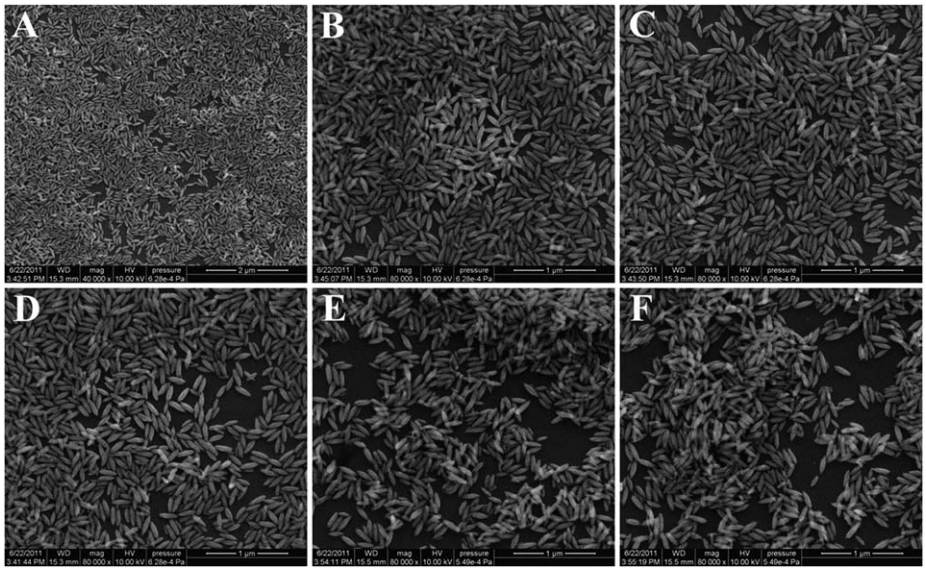

Fig. 2 (A) Low-magnification and (B) high-magnification FESEM images of rice-shaped $NaNdF_4$ nanoparticles; FESEM images of rice-shaped (C) $NaSmF_4$, (D) $NaEuF_4$, (E) $NaTbF_4$, and (F) $NaHoF_4$ nanoparticles.

with a rice-shaped morphology and an average length of 200 nm. The estimated average diameter near the half length of the rice-shaped $NaNdF_4$ nanoparticles is about 56 nm. The aspect ratio of about 3.6 : 1 is calculated from a number of $NaNdF_4$ nanoparticles. Interestingly, when this approach was applied to synthesize other rare-earth fluorides, it also produced a new class of important fluorides, as shown in Fig. 2C–F. The particle size and shape of the as-prepared respective $NaSmF_4$, $NaEuF_4$, $NaTbF_4$, and $NaHoF_4$ nanoparticles remain almost the same. The detailed particle size values are shown in Fig. S1.† More importantly, these uniform rice-shaped $NaLnF_4$ nanoparticles can be readily obtained in high amount through the present method. Furthermore, with these monodispersed rice-shaped $NaLnF_4$ nanoparticles as the template it will be very easy to sputter Ag NPs onto the surface of $NaLnF_4$, and further to form a large quantity of efficient SERS 'hot spots'.

3.2. The morphology evolution of the silver-decorated $NaLnF_4$ nanorices

For magnetron sputtering, it is revealed that the sputtering times and powers are critical to the morphologies of the resultant products. The hybrid nanorice particles prepared at a power of 50 W for different sputtering times are shown in Fig. 3. Varying the sputtering times from 10 to 150 s resulted in different sizes and surface fine structures of the products. For example, at a short time of 10 s, isolated silver nanoparticles with a particle size ranging from 16 to 32 nm were deposited on the surface of the fluoride nanorice (Fig. 3A). Increasing the sputtering time to 30 s, fluoride nanorice particles were covered by a thin silver shell with a thickness of about 3.0 nm. With prolonging of the sputtering time, the length and shell thickness of the nanorice correspondingly increased. The detailed values of these parameters were shown in Table S1.† It was found that a longer sputtering time resulted in a thicker silver shell and a rougher surface structure which might provide abundant efficient 'hot spots' to perform SERS detection and identification of analytes. However, further increase of the sputtering time to 150 s produced adhesive nanorice composites in the form of 'side by side' and 'tip by tip' aggregates. Because the tips of the nanorice connected with each other, the morphology of the original nanorice was deformed and the length and diameter of the nanorice became no longer obvious. Overall, the aspect ratio of the hybrid nanorice decreased with sputtering time increase. In the same way, we found that silver-decorated $NaLnF_4$ hybrid nanorice particles could also be realized by changing the sputtering power. When the sputtering time was fixed for 30 s, increasing the sputtering power from 30 to 150 W resulted in a wider diameter and longer length of the hybrid nanorice particles (Fig. 4). The values of these parameters were shown in Table S2.† From Fig. 3 and 4, we observed that the morphology evolution processws of the hybrid nanorice prepared under both sets of conditions were very similar to each other.

3.3. Extinction spectra of the $NaLnF_4$–Ag hybrid nanorice

Fig. 5 and S2† show the measured UV/vis spectra for the $NaLnF_4$–Ag nanorice particles with varying aspect ratio (R) values. Due to their anisotropy, the UV/vis spectra taken from the nanorice are characterized by two peaks in the range of 300–1000 nm, which are caused by transverse and longitudinal plasmon resonance, respectively.[36,37] Unlike the pure silver nanorice particles (with transverse and longitudinal plasmon bands around 400 and 900 nm, respectively), the as-prepared $NaLnF_4$–Ag hybrid nanorice in the present work display a transverse SPR peak around 420 nm and a longitudinal absorbance band at a wavelength range from 740 to 860 nm. As expected, a mild red-shift of the transverse SPR peak is observed with increasing aspect ratio. However, the longitudinal absorbance band remains almost unchanged. The appearance of the broad longitudinal absorbance band may originate from the formation of an incomplete core–shell structure of the hybrid nanorice. However,

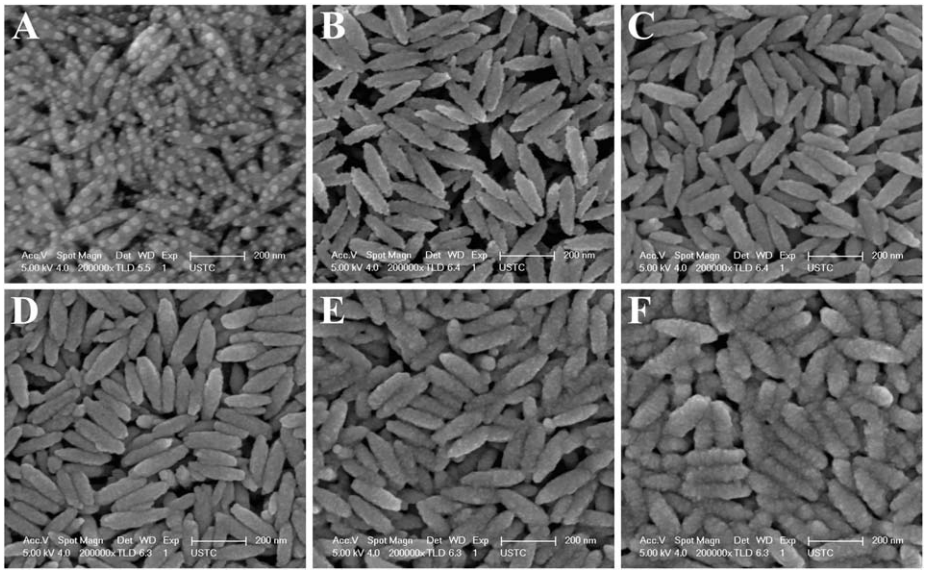

Fig. 3 FESEM images of $NaSmF_4$–Ag hybrid nanorice fabricated at a power of 50 W for different sputtering times: (A) 10 s, (B) 30 s, (C) 60 s, (D) 90 s, (E) 120 s and (F) 150 s.

the broad longitudinal absorbance band is insensitive to the variation of aspect ratios. Consequently, the longitudinal absorbance band is barely influenced by the aspect ratios.

3.4. SERS performances of the $NaLnF_4$–Ag hybrid nanorice

We evaluated their potential application as SERS substrates by using R6G, Mpy, and MBA as model Raman probes, respectively. Fig. 6A shows the SERS spectra of R6G adsorbed on $NaSmF_4$–Ag nanorice substrates prepared at different sputtering times. The peaks from 700 to 1700 cm^{-1} are attributed to R6G signals; vibrations at 1182, 1309, 1362, 1507, and 1651 cm^{-1} are assigned to C–H in-plane bending, C–O–C stretching, and C–C stretching of the aromatic ring.[38] Even a low concentration of R6G can produce a clear enhanced effect at 1651 cm^{-1}, which is one of the main characteristic bands.[39] For nanorice prepared with a 10 s sputtering time, the SERS intensity is the lowest, since only sparse silver nanoparticles were decorated on the surface of the $NaSmF_4$ nanorice particles (Fig. 3A). Obviously, the SERS intensity increases with the increase of sputtering time and reaches a maximal value for 120 s, then decreases to some extent for a longer sputtering time. The reason can be explained by the fact that the silver thickness and the number of silver nanoparticles increases with prolonged sputtering time which tends to form a large number of gaps or voids, providing more active sites which afford potential high density 'hot spots' to amplify the local electromagnetic fields as well as the Raman signal.[40] With further increase of the sputtering time, however, the nanorice particles

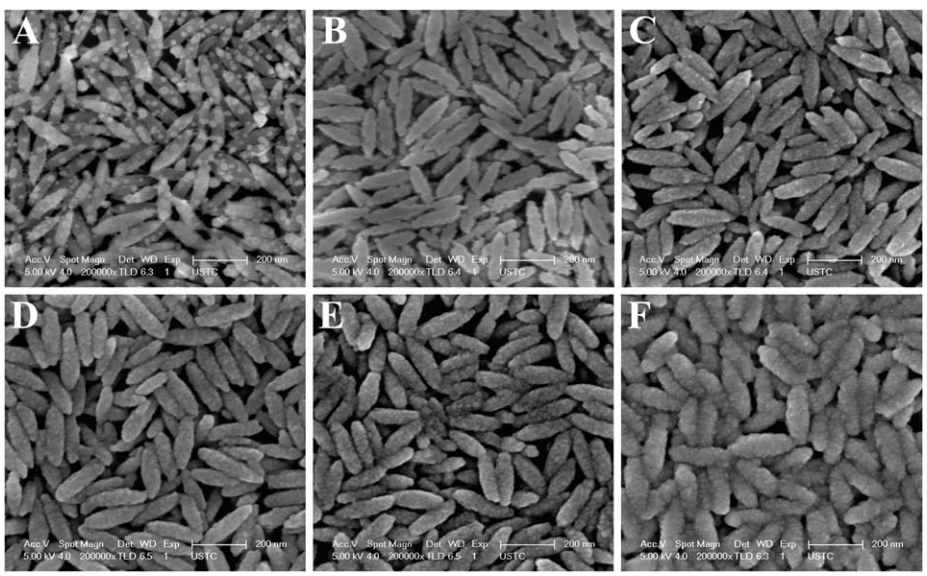

Fig. 4 FESEM images of $NaSmF_4$–Ag hybrid nanorices synthesized at different sputtering powers for 30 s: (A) 30 W, (B) 50 W, (C) 70 W, (D) 90 W, (E) 120 W and (F) 150 W.

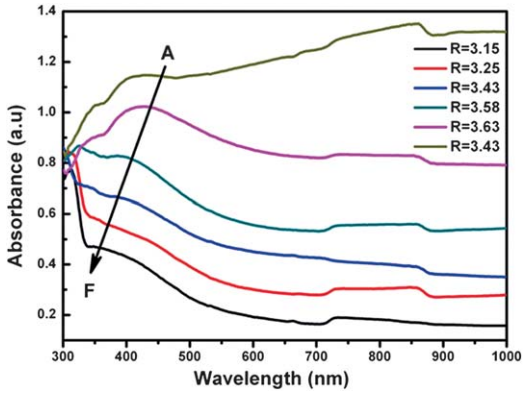

Fig. 5 UV/vis extinction spectra of the samples prepared at 50 W for different times: (A) 10 s, (B) 30 s, (C) 60 s, (D) 90 s, (E) 120 s and (F) 150 s; where *R* is the aspect ratio of the nanorice particles.

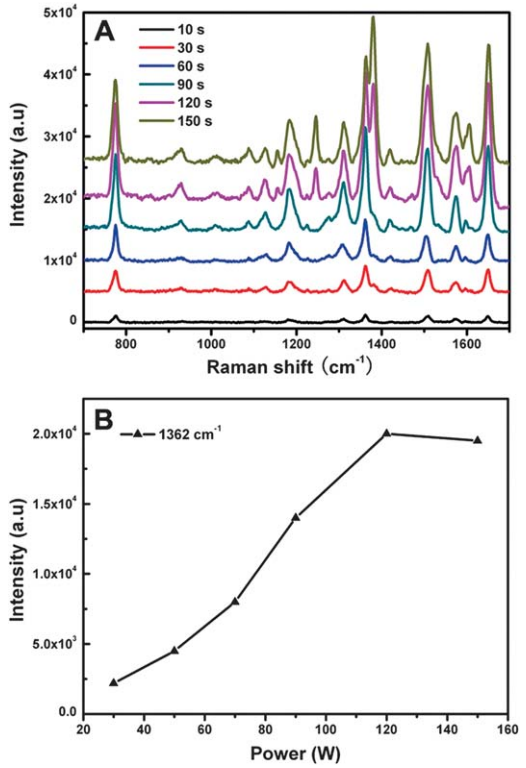

Fig. 6 SERS spectra of R6G (5×10^{-8} M) adsorbed on (A) $NaSmF_4$–Ag nanorice substrates prepared at various sputtering times, and (B) the relationship between SERS intensity and sputtering power ranging from 30 to 150 W.

deformed and the gaps or voids were filled by Ag NPs which leads to the decrease of potential 'hot spots', thus decreasing the SERS intensity. Fig. 6B shows the relationship between the SERS intensity (1362 cm^{-1}) and sputtering power ranging from 30 to 150 W. The detailed intensity and sputtering power values are given in Table S3.† It can be seen that the effects of sputtering power on the Raman performance were similar to those of sputtering time.

It is found that rare-earth fluorides as templates are suitable and readily enable the fabrication of $NaLnF_4$–Ag hybrid nanorice particles with desired SERS performances. Fig. 7 displays the SERS spectra of R6G adsorbed on five different $NaLnF_4$–Ag (Ln = Nd, Sm, Eu, Tb, Ho) nanorice substrates. Since the size and morphology of the fluorides are almost the same the produced $NaLnF_4$–Ag nanorice particles have similar roughness and nanoscale surface structure, thus leading to the same magnitude of SERS enhancement. Naturally, the five different $NaLnF_4$–Ag nanorice types exhibit a comparative enhancement efficiency. In these cases, we find that the Raman spectra can be ascribed to the R6G molecular signal and no intrinsic Raman signals of the fluorides are detected. Due to the lower excitation power of 0.5 mW and the short integration time of 6 s used in the testing process, it is not sufficient to excite the intrinsic Raman signals of the fluorides. Also, the fluorescence disturbance from the fluorides is not observed in the experiments. This may be due to the following facts. First, such a low excitation energy can effectively avoid auto-fluorescence from samples. To confirm this point, we measured the Raman spectra of pure fluoride nanorice particles. Fig. S3† shows the Raman spectra of pure $NaLnF_4$ (Ln = Nd, Sm, Eu, Tb, Ho) nanorice assembled on silicon wafers. It is clear that there is no fluorescence emission of $NaLnF_4$, and the two main peaks are attributed to silicon wafer signals. Second, the formation of the Ag shell greatly suppresses the fluorescence emission. These results indicate that fluorides as templates to prepare the $NaLnF_4$–Ag hybrid nanorice with expected SERS properties are shown to be a feasible and alternative strategy.

Recently, single-molecule detection by SERS with high sensitivity and molecular specificity based on metal nanomaterials has generated great interest.[41] In this study, preparation of $NaSmF_4$–Ag hybrid nanorice by the optimum procedure was used for the SERS mapping and enhancement factor calculation. The produced $NaSmF_4$–Ag hybrid nanorice significantly reduce the detection limit of R6G to 10^{-17} M. Well-defined Raman signals of R6G are demonstrated in Fig. 8A. The spectral intensities and resolutions are decreased with diluting the concentrations of the target molecules. It is found that additional R6G peaks still appeared at about 1509 and 1651 cm^{-1} at the extremely low concentration of 5×10^{-17} M; thus, it can be used as a 'fingerprint' for the detection of R6G. A SERS spatial map composed

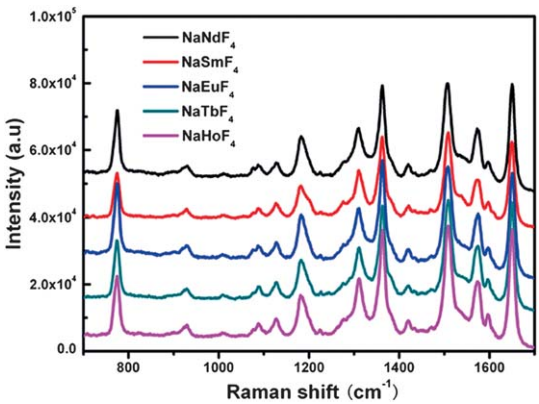

Fig. 7 SERS spectra of R6G (5×10^{-8} M) adsorbed on different $NaLnF_4$–Ag nanorice substrates. All the $NaLnF_4$–Ag nanorice particles were prepared at the same sputtering power of 50 W and a sputtering time of 120 s.

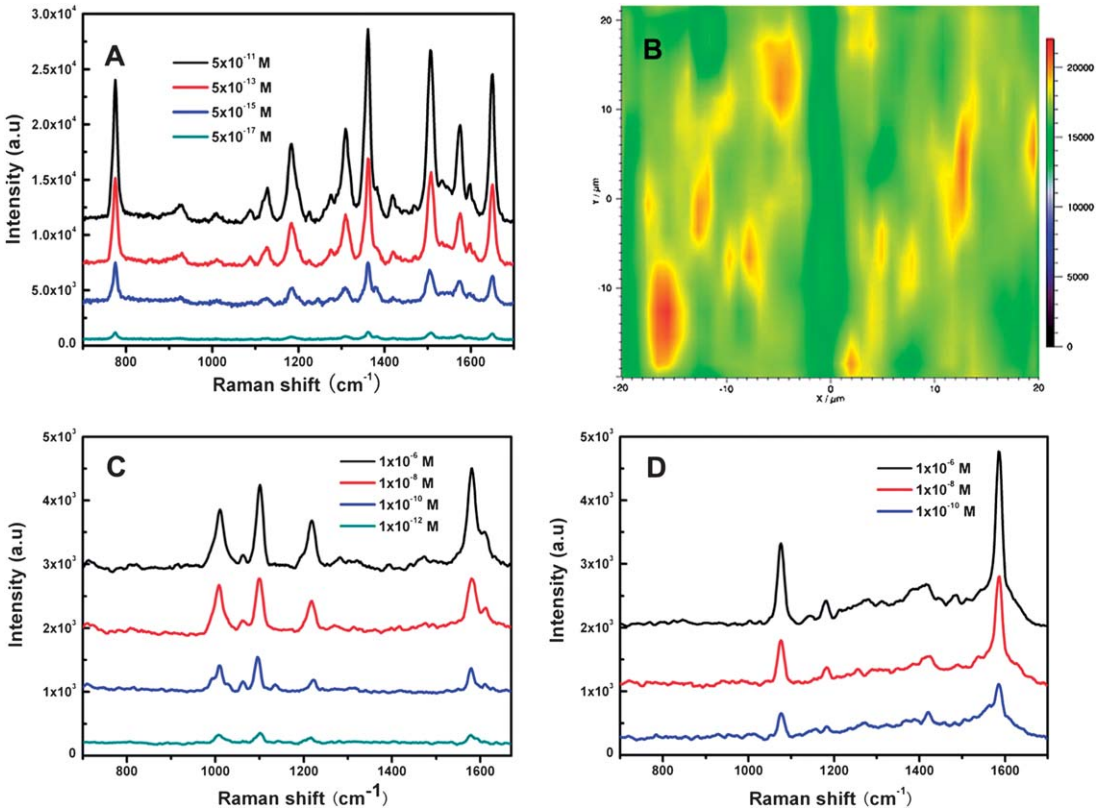

Fig. 8 SERS spectra obtained from different concentrations of R6G (A), Mpy (C), and MBA (D) adsorbed on $NaSmF_4$–Ag nanorice substrate; (B) SERS map (40 μm × 40 μm) of the 1362 cm^{-1} band of R6G observed from $NaSmF_4$–Ag substrate.

of the intensity of the 1362 cm^{-1} band of R6G adsorbed on the $NaSmF_4$–Ag substrate is shown in Fig. 8B. It can be seen that there is a homogeneous SERS response throughout the whole surface, with a scale of 40 μm. Except for some inevitable defect spots, most of them are between 180 00 and 200 00 counts with a relatively narrow distribution within 10% deviation from the mean, which shows that our $NaSmF_4$–Ag hybrid nanorice is an excellent SERS substrate. In addition to the strong SERS enhancement effect, the $NaSmF_4$–Ag nanorice particles are stable and can be produced with high repeatability, which shows great potential application for universal SERS substrates.

Furthermore, when the as-obtained nanorice substrate was applied for the detection of Mpy molecules, it also exhibited high detection sensitivity and the detection concentration was as low as 10^{-12} M. Fig. 8C shows the SERS spectra of Mpy with different concentrations adsorbed on the $NaSmF_4$–Ag substrate. The major bands from 700 to 1700 cm^{-1} are attributed to Mpy signals. The bands at 1009, 1219 and 1582 cm^{-1} are assigned to the ring-breathing modes, CH/NH deformation modes and pyridine ring C=C stretch modes, respectively.[42] The band at 1101 cm^{-1} belongs to so-called X-sensitive modes that are described as modes strongly coupled between the substitute and aromatic ring modes.[43] Additionally, MBA was used to further demonstrate the detection sensitivity of the $NaLnF_4$–Ag substrates. The SERS spectra of MBA with different concentrations adsorbed on the $NaSmF_4$–Ag substrates are shown in Fig. 8D. The two strong SERS peaks appearing at 1075 and 1584 cm^{-1} are assigned to ν_{8a} and ν_{12} aromatic ring vibrations, respectively; other weak bands around 1150 and 1184 cm^{-1} are attributed to the C–H deformation modes.[44] It is observed that three obvious SERS bands can still be detected in concentration ranges down to 10^{-10} M. These observations confirm that this kind of $NaLnF_4$–Ag nanorice substrate can achieve the ultra-trace detection of analytes.[45]

Generally, it is believed that many factors simultaneously contribute to the Raman enhancement effect:[46] an electromagnetic effect associated with large local fields due to resonances occurring in the nanostructures on the metal surface, and a chemical effect involving a scattering process associated with chemical interaction between the molecule and the metal surface. The chemical effect, however, does not lead to strong electronic coupling with the surface plasmon; therefore, the SERS response mainly results from an electromagnetic enhancement. The electromagnetic effect is believed to be a few orders of magnitude greater than that due to the chemical effect. Moreover, in the rare-earth fluoride luminescent materials decorated with the Au or Ag system, the fluoride nanomaterials can serve as the energy donor and metal nanoparticles as the receptor. Luminescence resonance energy transfer of rare-earth fluorides to metal nanoparticles has been observed in many researches.[29,47–49] Consequently, these $NaLnF_4$–Ag hybrid nanorice substrates can achieve such high enhancement efficiency for R6G, Mpy, and MBA.

In the present study, it is very difficult to estimate the exact number of molecules covered by the laser spot. Thus, it is not easy to calculate an accurate EF. However, we can roughly

estimate the enhancement factor obtained from R6G, Mpy and MBA. To determine the SERS enhancement abilities of the $NaLnF_4$–Ag nanorice substrates, we first estimated the EF of R6G on the $NaSmF_4$–Ag nanorice substrates. The intensity of the vibrations at the 1362 cm^{-1} band of the aromatic ring was chosen to estimate the EF of the substrates using the following expression:

$$EF = (I_{surf}/I_{bulk})(N_{bulk}/N_{surf})$$

where N_{bulk} is the number of analyte molecules in the focal volume and I_{bulk} is the intensity of the Raman signal as calculated from the peak area of the 1362 cm^{-1} band for spectra taken of the analyte on a bare glass slide, whereas N_{surf} and I_{surf} are the same parameters when the SERS substrate is utilized. The Raman spectrum of an aqueous R6G solution (5 μL, 2 mM) was used for calculation of the EF. For the 'bulk' values, R6G solution was dropped on a silicon wafer, which formed a spreading area of 5 mm in diameter. The intensity I_{bulk} at 1362 cm^{-1} is 762 (see ESI Fig. S4†). The I_{surf} at 1362 cm^{-1} could be obtained from Fig. 8A (10^{-17} M R6G) to be 609. Since both N_{surf} and N_{bulk} are mainly determined by the concentration under the given volume and area, it was considered that the ratio of N_{bulk} to N_{surf} could be estimated from the ratio of the concentrations.[50] Accordingly, the present substrate achieved a very high Raman EF of 3.2×10^{13}. The EF values for R6G absorbed on different $NaLnF_4$–Ag substrates were calculated with the equation mentioned above and are given in Table S4.† Similarly, the probe molecules of Mpy and MBA are analyzed and the present substrate achieves very high Raman EF values of $\sim 10^{11}$ and 10^9, respectively. The reduction in the EF between the R6G and Mpy/MBA is most likely due to the laser used for the SERS measurement. The 532 nm excitation source is very close to the λ_{max} of R6G ($\sim$530 nm), and the SERS observed is in fact surface enhanced resonant Raman scattering (SERRS). The resonant condition results in an increase of 2–4 orders of magnitude enhancement, which is consistent with the greater than three orders of magnitude difference between R6G and Mpy/MBA. Due to their excellent SERS performances, we believe that such hybrid $NaLnF_4$–Ag nanorice particles serving as great and universal SERS substrates are likely to be employed to detect other ultratrace biomolecules or dangerous chemicals.

4. Conclusions

In summary, we have designed a simple and efficient template synthesis of $NaLnF_4$–Ag hybrid nanorice particles by a magnetron sputtering method. The obtained hybrid nanorice substrates were characterized by TEM, FE-SEM, and UV/vis. The thickness, surface feature, and morphology of the silver-decorated $NaLnF_4$ nanorice particles could be precisely controlled by adjusting the magnetron sputtering parameters. It is important to note that the $NaLnF_4$–Ag nanorice particles were stable and could be produced with high repeatability, which showed great potential application for universal SERS substrates. The detection limits for R6G, Mpy, and MBA of the optimized $NaLnF_4$–Ag nanorice substrates approached 10^{-17} M, 10^{-12} M, and 10^{-10} M, respectively. A higher Raman enhancement factor of 10^{13} for R6G was achieved, thus allowing this kind of substrate to be sensitive enough for single-molecule detection. We believe that such hybrid nanorice particles can serve as ideal substrates for SERS applications and provide an excellent candidate for SERS analysis.

Acknowledgements

This work was supported by the National Natural Science Foundation of China (no. 20873153), the National Basic Research Program of China (2011CB302103), the State Key Laboratories of Transducer Technology (Skt0906), the Special Foundation of China Postdoctoral Science Foundation (201104316), and the China Postdoctoral Science Foundation Funded Project (2011M501408) for financial support.

References

1 S. Lal, N. K. Grady, J. Kundu, C. S. Levin, J. B. Lassiter and N. J. Halas, *Chem. Soc. Rev.*, 2008, **37**, 898–911.
2 S. Y. Lee, L. Hung, G. S. Lang, J. E. Cornett, I. D. Mayergoyz and O. Rabin, *ACS Nano*, 2010, **4**, 5763–5772.
3 X. H. Xia, J. Zeng, B. McDearmon, Y. Q. Zheng, Q. G. Li and Y. N. Xia, *Angew. Chem., Int. Ed.*, 2011, **50**, 12542–12546.
4 L. Su, W. Z. Jia, D. P. Manuzzi, L. C. Zhang, X. P. Li, Z. Y. Gu and Y. Lei, *RSC Adv.*, 2012, **2**, 1439–1443.
5 Y. C. Lai, W. X. Pan, D. J. Zhang and J. H. Zhan, *Nanoscale*, 2011, **3**, 2134–2137.
6 N. P. W. Pieczonka and R. F. Aroca, *Chem. Soc. Rev.*, 2008, **37**, 946–954.
7 P. Etchegoin, R. C. Maher, L. F. Cohen, H. Hartigan, R. J. C. Brown, M. J. T. Milton and J. C. Gallop, *Chem. Phys. Lett.*, 2003, **375**, 84–88.
8 G. C. Schatz, M. A. Young and R. P. Van Duyne, *Top. Appl. Phys.*, 2006, **103**, 19–45.
9 C. Y. Song, J. Chen, J. L. Abell, Y. P. Cui and Y. P. Zhao, *Langmuir*, 2012, **28**, 1488–1495.
10 Y. G. Sun and Y. N. Xia, *Science*, 2002, **298**, 2176–2179.
11 A. Gutés, C. Carraro and R. Maboudian, *J. Am. Chem. Soc.*, 2010, **132**, 1476–1477.
12 Y. G. Sun, *Nanoscale*, 2010, **2**, 1626–1642.
13 M. F. Zhang, A. W. Zhao, H. Y. Guo, D. P. Wang, Z. B. Gan, H. H. Sun, D. Li and M. Li, *CrystEngComm*, 2011, **13**, 5709–5717.
14 H. Y. Liang, Z. P. Li, W. Z. Wang, Y. S. Wu and H. X. Xu, *Adv. Mater*, 2009, **21**, 4614–4618.
15 M. F. Zhang, A. W. Zhao, H. H. Sun, H. Y. Guo, D. P. Wang, D. Li, Z. B. Gan and W. Y. Tao, *J. Mater. Chem.*, 2011, **21**, 18817–18824.
16 H. Wang, D. W. Brandl, F. Le, P. Nordlander and N. J. Halas, *Nano Lett.*, 2006, **6**, 827–832.
17 X. Xu and M. B. Cortie, *J. Phys. Chem. C*, 2007, **111**, 18135–18142.
18 L. Chen, H. K. Seo, Z. Mao, Y. M. Jung and B. Zhao, *Anal. Methods*, 2011, **3**, 1622–1627.
19 M. C. Moulton, L. K. Braydich-Stolle, M. N. Nadagouda, S. Kunzelman, S. M. Hussain and R. S. Varma, *Nanoscale*, 2010, **2**, 763–770.
20 M. N. Nadagouda and R. S. Varma, *Green Chem.*, 2007, **9**, 632–637.
21 B. M. Teo, S. K. Suh, T. A. Hatton, M. Ashokkumar and F. Grieser, *Langmuir*, 2011, **27**, 30–33.
22 P. Kundu, C. Nethravathi, P. A. Deshpande, M. Rajamathi, G. Madras and N. Ravishankar, *Chem. Mater.*, 2011, **23**, 2772–2780.
23 D. Amans, C. Malaterre, M. Diouf, C. Mancini, F. Chaput, G. Ledoux, G. Breton, Y. Guillin, C. Dujardin, K. Masenelli-Varlot and P. Perriat, *J. Phys. Chem. C*, 2011, **115**, 5131–5139.
24 L. H. Lu, A. Kobayashi, K. Tawa and Y. Ozaki, *Chem. Mater.*, 2006, **18**, 4894–4901.
25 J. Zhang, X. H. Liu, L. W. Wang, T. L. Yang, X. Z. Guo, S. H. Wu, S. Y. Wang and S. M. Zhang, *J. Phys. Chem. C*, 2011, **115**, 5352–5357.
26 L. Chen, H. K. Seo, Z. Mao, Y. M. Jung and B. Zhao, *Anal. Methods*, 2011, **3**, 1622–1627.
27 S. Deng, H. M. Fan, X. Zhang, K. P. Loh, C. L. Cheng, C. H. Sow and Y. L. Foo, *Nanotechnology*, 2009, **20**, 175705–175710.
28 H. B. Tang, G. W. Meng, Q. Huang, Z. Zhang, Z. L. Huang and C. H. Zhu, *Adv. Funct. Mater.*, 2012, **22**, 218–224.

29 W. Feng, L. D. Sun and C. H. Yan, *Chem. Commun.*, 2009, 4393–4395.
30 W. Xu, X. Bai, S. Xu, Y. S. Zhu, L. Xia and H. W. Song, *RSC Adv.*, 2012, **2**, 2047–2054.
31 J. P. Zhang, C. C. Mi, H. Y. Wu, H. Q. Huang, C. B. Mao and S. K. Xu, *Anal. Biochem.*, 2012, **421**, 673–679.
32 G. F. Wang, Q. Peng and Y. D. Li, *Acc. Chem. Res.*, 2011, **44**, 322–332.
33 H. Zhang, Y. J. Li, I. A. Ivanov, Y. Q. Qu, Y. Huang and X. F. Duan, *Angew. Chem., Int. Ed.*, 2010, **49**, 2865–2868.
34 S. Schietinger, T. Aichele, H. Q. Wang, T. Nann and O. Benson, *Nano Lett.*, 2010, **10**, 134–138.
35 M. F. Zhang, H. Fan, B. J. Xi, X. Y. Wang, C. Dong and Y. T. Qian, *J. Phys. Chem. C*, 2007, **111**, 6652–6657.
36 B. J. Wiley, Y. Chen, J. M. Mclellan, Y. Xiong, Z. Y. Li, D. Ginger and Y. N. Xia, *Nano Lett.*, 2007, **7**, 1032–1036.
37 H. Y. Liang, H. X. Yang, W. Z. Wang, J. Q. Li and H. X. Xu, *J. Am. Chem. Soc.*, 2009, **131**, 6068–6069.
38 L. L. Sun, Y. H. Song, L. Wang, C. L. Guo, Y. J. Sun, Z. L. Liu and Z. Li, *J. Phys. Chem. C*, 2008, **112**, 1415–1422.
39 P. Hildebrandt and M. Stockburger, *J. Phys. Chem.*, 1984, **88**, 5935–5939.
40 J. Rodríguez-Fernández, A. M. Funston, J. Pérez-Juste, R. A. Álvarez-Puebla, L. M. Liz-Marzán and P. Mulvaney, *Phys. Chem. Chem. Phys.*, 2009, **11**, 5909–5914.
41 A. Gutés, C. Carraro and R. Maboudian, *J. Am. Chem. Soc.*, 2010, **132**, 1476–1477.
42 H. L. Hu, W. Song, W. D. Ruan, Y. F. Wang, X. Wang, W. Q. Xu and B. Zhao, *J. Colloid Interface Sci.*, 2010, **344**, 251–255.
43 W. Song, Y. X. Wang and B. Zhao, *J. Phys. Chem. C*, 2007, **111**, 12786–12791.
44 A. Michota and J. Bukowska, *J. Raman Spectrosc.*, 2003, **34**, 21–25.
45 L. H. Qian, X. Q. Yan, T. Fujita, A. Inoue and M. W. Chen, *Appl. Phys. Lett.*, 2007, **90**, 153120–153122.
46 M. W. Shao, L. Lu, H. Wang, S. Wang, M. L. Zhang, D. D. D. Ma and S. T. Lee, *Chem. Commun.*, 2008, 2310–2312.
47 C. C. Mi, H. Y. Gao, F. Li and S. K. Xu, *Colloids Surf., A*, 2012, **395**, 152–156.
48 L. R. P. Kassab, F. A. Bomfim, J. R. Martinelli, N. U. Wetter and J. J. Neto, *Appl. Phys. B: Lasers Opt.*, 2009, **94**, 239–242.
49 V. Rai, L. Menezes, C. de Araújo, L. Kassab, D. da Silva and R. Kobayashi, *J. Appl. Phys.*, 2008, **103**, 093526–093530.
50 X. T. Wang, W. S. Shi, G. W. She, L. X. Mu and S. T. Lee, *Appl. Phys. Lett.*, 2010, **96**, 053104–053106.

